RSC Advances

PAPER

View Article Online
View Journal | View Issue

Cite this: *RSC Adv.*, 2020, **10**, 8172

Preparation of activated carbon nanofibers using degradative solvent extraction products obtained from low-rank coal and their utilization in supercapacitors†

Weixiang Qian,[ab] Xian Li,[*abc] Xianqing Zhu,[b] Zhenzhong Hu,[b] Xu Zhang,[b] Guangqian Luo[b] and Hong Yao[b]

In this study, low-rank coal was separated into three solid fractions by a degradative solvent extraction method. The high-molecular-weight extract (termed Deposit) had some outstanding properties such as high carbon content, almost no ash, high aromaticity, good thermoplasticity and high solubility in DMF. Therefore, Deposit with some proportion of polyacrylonitrile (PAN) was used to prepare activated carbon nanofibers by electrospinning and CO_2 activation. Moreover, the utilization of these carbon nanofibers as a supercapacitor electrode was preliminarily investigated. The results showed that the specific surface area of the Deposit-based carbon nanofibers (1005 $m^2\ g^{-1}$) was significantly higher than that of the nanofibers obtained from pure PAN (688 $m^2\ g^{-1}$). TGA simulations showed that this was caused by the different thermal decomposition behaviors of Deposit and PAN during the stabilization and activation processes. In addition, the Deposit-based carbon nanofibers showed a better specific capacitance (192.6 F g^{-1} at 1 A g^{-1}) and cycling performance (retention rate of 89.8% after 1000 cycles at 5 A g^{-1}) in a 6 M KOH electrolyte. The factors, such as the enhanced surface area and pore volume and decreased average fiber diameter, affected the electrochemical properties of the carbon nanofibers. Thus, it has been proven that the high-molecular-weight extract obtained from low-rank coal by degradative solvent extraction is a promising precursor for the preparation of carbon nanofibers with unique electrochemical properties.

Received 28th November 2019
Accepted 6th February 2020

DOI: 10.1039/c9ra09966b

rsc.li/rsc-advances

Introduction

Porous carbon materials, such as activated carbon, graphene, and activated carbon nanofibers, have many advantages such as high specific surface areas, electrical conductivity and stable structures. Thus, they are widely used in the preparation of double-layer supercapacitor electrodes.[1,2] Among various carbon materials, activated carbon is most widely used in supercapacitors due to its high surface area and lower cost.[3] However, during the supercapacitor preparation process, a complicated process is required to form electrodes from powdered activated carbons. Furthermore, the preparation process needs the addition of a binder, which increases the resistance and dead weight, lowering the supercapacitor performance.[4] Recently, carbon nanofibers, as promising materials for supercapacitor electrodes, have attracted significant attention due to their nanoscale diameter, large specific surface area, and suitable pore size.

Moreover, compared to activated carbons, carbon nanofibers can be directly used as electrodes due to their self-sustaining nature; this avoids the complex preparation process of electrodes.[5–7]

Electrospinning has been widely used for preparing carbon nanofibers due to its simple process and easy experimental controllability. The fiber structure can be directly controlled by adjusting parameters such as voltage and distance.[8,9] However, due to limited spinnability and yield, most of the precursors used in this process are organic polymers such as polyacrylonitrile (PAN),[10–12] polyvinyl alcohol (PVA),[13] and polybenzimidazole (PBI).[14] It is believed that the quality of the carbon fibers used for the preparation of supercapacitor electrodes significantly depends on the structure, assembly and alignment of aromatic constituents. In general, pitch-based carbon fibers typically provide better electrochemical

[a]China School of China-EU Institute for Clean and Renewable Energy, School of Energy and Power Engineering, Huazhong University of Science and Technology, Wuhan 430074, People's Republic of China. E-mail: xian_li@hust.edu.cn; Tel: +86-27-87545526

[b]State Key Laboratory of Coal Combustion, Huazhong University of Science and Technology, Wuhan 430074, China

[c]Key Laboratory of Coal Clean Conversion and Chemical Process Autonomous Region, College of Chemistry and Chemical Engineering, Xinjiang University, Urumqi 830000, Xinjiang, China

† Electronic supplementary information (ESI) available. See DOI: 10.1039/c9ra09966b

properties than the carbon fibers obtained from hard carbons such as PAN.[15] Yang *et al.*[16] produced PAN-, pitch-, PBI-, and polyimide (PI)-derived carbon nanofibers by electrospinning. Moreover, the nanofibers obtained from pitch exhibited the highest specific surface area and carbon yield and excellent electrical conductivity, showing their potential in energy storage. However, the application of pitch as a precursor is usually limited by some problems such as difficulty in the preparation of concentrated solutions because pitch contains complex components and a rare solvent can completely dissolve the pitch. Another challenge is to find a solvent with proper boiling point to produce solidified fibers. Thus, a complex pretreatment is usually required to remove the volatile small molecules and larger molecular solids from pitch before electrospinning.[17,18] Some researchers have used DMF extracts of coal as a precursor for the preparation of nanofibers by electrospinning. However, raw coal needs to be pretreated because of its rather low solubility in DMF. Moreover, the raw coal pretreated using strong acid solutions, such as H_2SO_4, HNO_3, and $KMnO_4$, has small application prospects.[19,20]

Recently, we reported a degradative solvent extraction method. The low rank-coal can be converted into three solid fractions in a non-polar solvent under a relatively mild condition (around 350 °C).[21–23] Moreover, the non-polar solvent can be easily recycled.[24] The products included solid products, which were high-molecular-weight extracts (Deposit), low-molecular-weight extracts (Soluble) and residues (Residues), and by-products, which were liquid (mainly H_2O) and gaseous products (mainly CO_2). In our previous studies, the utilization of these three products has been investigated for different purposes.[25–28] Deposit was obtained with a yield of around 15%, carbon content of about 80–85%, and almost no ash and moisture. Its softening point ranged from 190 °C to 270 °C.[21] Moreover, due to the deoxygenation reaction and aromatization reaction during the extraction process, the aromaticity of Deposit increased after extraction. These characteristics are similar to those of pitch; however, Deposit has a narrower molecular weight range of around 500.[21] Furthermore, Deposit can be easily dissolved in organic solvents, such as DMF, as compared to raw coal and pitch. This can solve the problem of low solubility of pitch in DMF. Yang *et al.*[29] successfully prepared carbon fibers using HyperCoal as a precursor by a melt-spinning method. HyperCoal was obtained *via* coal extraction using a non-polar solvent at a temperature below 400 °C. It was similar to the mixture of Soluble and Deposit and thus had a wider molecular weight range and thermoplastic temperature range. Thus, similar to pitch, HyperCoal also needed complex pretreatment.

Previous studies indicate that Deposit should be a proper precursor for the preparation of carbon nanofibers using the electrospinning method. Thus, in this study, Deposit was used as a precursor for the fabrication of carbon nanofibers for the first time by the electrospinning method and CO_2 activation. Moreover, the possibility of using the Deposit-based carbon nanofibers as an electrode for supercapacitors was preliminarily studied.

Experimental

Degradative solvent extraction procedure

Subbituminous coal (obtained from Xinjiang, China) was used as a parent coal. Table 1 shows the results of the proximate and elemental analyses of raw coal and its derivatives. The raw coal was extracted at 350 °C in a specially designed autoclave using 1-methylnaphthalene (1-MN) as a solvent. Fig. 1 shows a schematic of the autoclave; the upper part is the reactor with a filter, and the bottom part is a reservoir. About 40 g dried coal powder (grain size: 200–300 mesh) and 400 ml 1-MN were added to the autoclave. The detailed experimental procedure has been described in our previous studies.[21–23] The autoclave was sealed, and the temperature was increased to 350 °C at the heating rate of 5 °C min^{-1} and maintained for 60 min followed by purging with N_2. The extracts with the solvent were flowed into the reservoir at the moment the experiment was completed by opening the valve, and the unextractable fraction (Residue) remained in the autoclave. After cooling down to room temperature, the precipitated solid fraction, named Deposit, was retrieved by filtration. The remaining extract dissolved in 1 MN was named Soluble and was obtained through evaporation at 120 °C to remove the solvent. After drying in vacuum at 150 °C for about 4 h to remove the residual 1-MN, the solid products Residue, Soluble, and Deposit were finally obtained.

Table 1 The results of the ultimate analysis and proximate analysis of raw coal and solid products

	Ultimate analysis (wt%, d.a.f.)				Proximate analysis (wt%, d.b)		
Sample	C	H	N	O[diff.]	VM[a]	ash	FC[b]
Raw coal	77.02	6.23	1.47	15.28	46.42	11.96	41.62
Soluble	81.20	7.41	0.91	10.48	93.22	0.00	6.78
Deposit	79.82	5.96	1.44	12.78	53.91	1.78	44.31
Residue	77.54	5.10	1.34	15.98	46.63	13.61	39.76

[a] VM, volatile matter. [b] FC, fixed carbon.

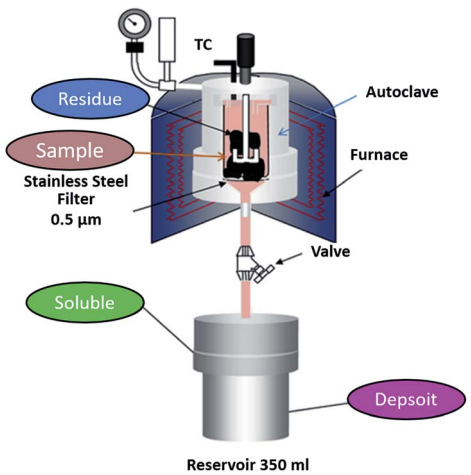

Fig. 1 Schematic of the autoclave.

Preparation of the Deposit/PAN composite nanofibers by electrospinning

PAN (M_w = 150 000) was obtained from Sigma-Aldrich. DMF (assay 99.5% min) was obtained from Shanghai Titan Scientific Co., Ltd, China.

Deposit has an aromatic ring structure and the molecular weight of only around 500. These factors made the pure Deposit hard to perform fiber structure during the electrospinning period. Thus, PAN with a long chain molecular structure is needed as a fiber skeleton to prepare carbon fibers. Therefore, PAN was added to Deposit at different ratios (PAN : Deposit = 2 : 1 and 1 : 1) in order to improve the spinnability of Deposit. The electrospinning solution was prepared by dissolving 1.5 g PAN/Deposit mixed powder in 11 ml DMF. To this solution, water was added followed by stirring for 2 h at 55 °C. The solution was used to fabricate nanofibers by an electrospinning device (SS-2325H, Ucalery Co., Ltd, China). A negatively charged and ground rotating collector was used to obtain the nanofibers. The spinning distance was fixed to 16 cm and the voltage was 22 V. The fabricated Deposit/PAN nanofibers were then placed in a tube furnace (OTF-1200X-S, Kejing Materials Technology Co. Ltd, China) for stabilization and carbonization. The stabilization temperature was increased to 280 °C at the heating rate of 0.5 °C min^{-1} in air and maintained for 2 h. After stabilization, the temperature was increased to 900 °C at the heating rate of 5 °C min^{-1} under an N_2 atmosphere. When the temperature reached 900 °C, the gas was changed to CO_2 and this temperature was maintained for 1 h for activation. Then, the fibers were cooled down to room temperature under an N_2 atmosphere. The obtained activated carbon nanofibers were named based on the mixing ratio of PAN and Deposit as ACFs (pure PAN), ACFs-2-1 (PAN : Deposit = 2 : 1) and ACFs-1-1 (PAN : Deposit = 1 : 1).

Material characterization

An elemental analyzer (Vario CHN EL-2) was used to analyze the elemental composition of the extracts and raw coal. Proximate analysis was conducted using a thermogravimetric analyzer (TGA, ELTRA TGA Thermostep) by the methods of GB/T212-2008. Chemical structure analysis was conducted by a Fourier transform infrared spectrometer (FTIR, Bruker VERTEX-70).

The simulations of the stabilization and activation processes were conducted by a thermogravimetric analyzer (TG, NETZSCH STA499-F3). The morphology of the nanofibers was investigated by scanning electron microscopy (SEM, Zeiss MERLIN compact). The pore structure measurement was conducted by N_2 adsorption isotherms at 77 K (BET, Quantachrome Autosorb-iQ). The surface area was obtained by applying the BET equation. The carbon structure of the nanofibers was determined by a Fourier transform Raman spectrometer (FT-Raman, Renishaw inVia reflex) and an X-ray diffractometer (XRD, Rigaku D-MAX 2500/PC).

Electrochemical measurements

All the prepared nanofibers were cut into 1 × 1 cm^2 pieces and directly used as the working electrode with no binders and conductive agent. The electrochemical properties were measured by a three-electrode workstation (Chenhua, CHI660E). An aqueous electrolyte (6 M KOH) was used, and a Pt foil and the Hg/HgO electrode were applied as the counter and reference electrodes, respectively. Cyclic voltammetry (CV) was performed at the scan rates of 5, 10, 20, 50, and 100 mV s^{-1} in the potential window ranging from −0.8 V to 0.1 V. Galvanostatic charge/discharge measurement (GCD) was performed at the current densities of 1, 2, 5, and 10 A g^{-1} in the same potential window. The specific capacitance was calculated at 1 A g^{-1}. Electrochemical impedance spectroscopy (EIS) was conducted in the frequency range from 100 kHz to 10 mHz at open circuit voltage with an AC amplitude of 5 mV.

Results and discussion

Yields and characterization of the extraction products

Fig. S1† shows the yields of the extraction products. It was found that the extraction products mainly consisted of solid products. Small amounts of liquid and gas products were formed during extraction, which are marked as "others" in Fig. S1.† The yields of the Soluble and Deposit products were 14.7% and 9.2%, respectively. In our previous study, the yield of Deposit reached 16.9%, and the decrease in the yield of Deposit in this study was caused by the different properties of raw coal.[21] Table 1 shows the results of the proximate and ultimate analyses of the solid fraction. The carbon content of Deposit increased to 79.8%, which was significantly higher than that of the raw coal, whereas its oxygen content was lower than 13%. This indicated that the deoxygenation reactions and "carbon enrichment" process occurred during the degradative solvent extraction process. Compared with raw coal, Deposit had more fixed carbon, which ensured high yields of carbon nanofibers during the subsequent thermal processes. Moreover, Soluble can be used for producing high-quality liquid fuels.[25] Residues have better performance in combustion and gasification[26,27] and are a precursor for activated carbon preparation.[28]

High ash contents in carbon nanofibers lead to leakage current and self-discharge and have a bad influence on the cycling performance. Although the ash content of the Deposit prepared in this study was as high as 1.78%, the ash contents of ACFs, ACFs-2-1, and ACFs-1-1 prepared in this study were only 0.1%, 0.4%, and 0.7%, respectively. These are relatively low and similar to the ash content of commercial carbon fibers, which is generally lower than 0.9%.[30] The low ash content in the carbon fiber prepared from Deposit is because the ash in Deposit has low solubility in DMF; this means that most of the ash settles in the spinning solution. Moreover, during the activation period, some of the ash in the fiber is released and displaced by the N_2 flow at high temperatures. Furthermore, the ash content of the Deposits prepared from other coals in our previous studies was as low as 0.25%.[21,24] This was due to the low ash content and different compositions of the raw coal.

The chemical structure characterization of Deposit and raw coal was conducted by FTIR spectroscopy. The spectra of Deposit and raw coal are obviously different, as shown in Fig. 2. The spectrum of raw coal has broader absorption bands at 3100–3500 cm^{-1}, corresponding to the O–H stretching

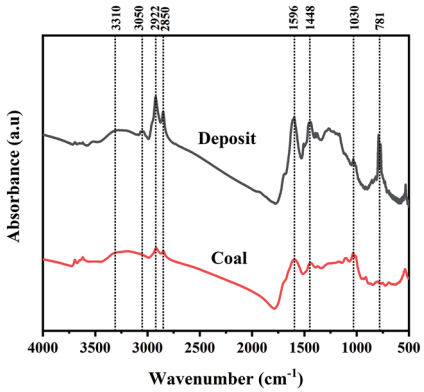

Fig. 2 FTIR spectra of Deposit and raw coal.

vibration, as compared to that of Deposit. The C–O stretching vibration peak (~1030 cm^{-1}) is weakened in the spectrum of Deposit. The distinct peaks appearing at 2850–2950 cm^{-1} are attributed to aliphatic C–H, C–H_2 and C–H_3 stretching vibrations. The aliphatic groups will increase the rate during the activation process.[31] Moreover, the enhancement in the intensity of the peaks attributed to aromatic groups can be observed in the spectrum of Deposit: aromatic C–H stretching vibration peaks at 3050 cm^{-1} and 781 cm^{-1} and aromatic C=C stretching vibration peaks at 1370–1650 cm^{-1}. This indicated that Deposit mainly consisted of aromatic hydrocarbons due to the deoxygenation and aromatization reactions occurring during the extraction process. The aromaticity of Deposit was calculated to be as high as 0.74 in our previous study.[21] It is widely acknowledged that materials with high aromaticity lead to high orientation and will have better performance in carbon fiber preparation.[31,32]

Fig. S2† shows the images of Deposit and raw coal dissolved in DMF for 48 h. It can be clearly observed that Deposit has better solubility in DMF. Wang *et al.*[20] used $KMnO_4$ to oxidize raw coal. The treated coal was more soluble in DMF because the large molecule was cut into small parts. During the degradative solvent extraction process, the three-dimensional structure of coal is gradually destroyed; moreover, aromatic hydrocarbons, which have excellent solubility in DMF, diffuse into the solvent and turn into Deposit.

Structural characterization of the prepared activated carbon fibers

Fig. 3 shows the scanning electron microscopy (SEM) images of the prepared activated carbon fibers. No fusion and bonding structures were found. The average diameter of ACF was about 300 nm and it had a relatively smooth surface. However, the average diameters of ACFs-2-1 and ACFs-1-1 were about 260 nm

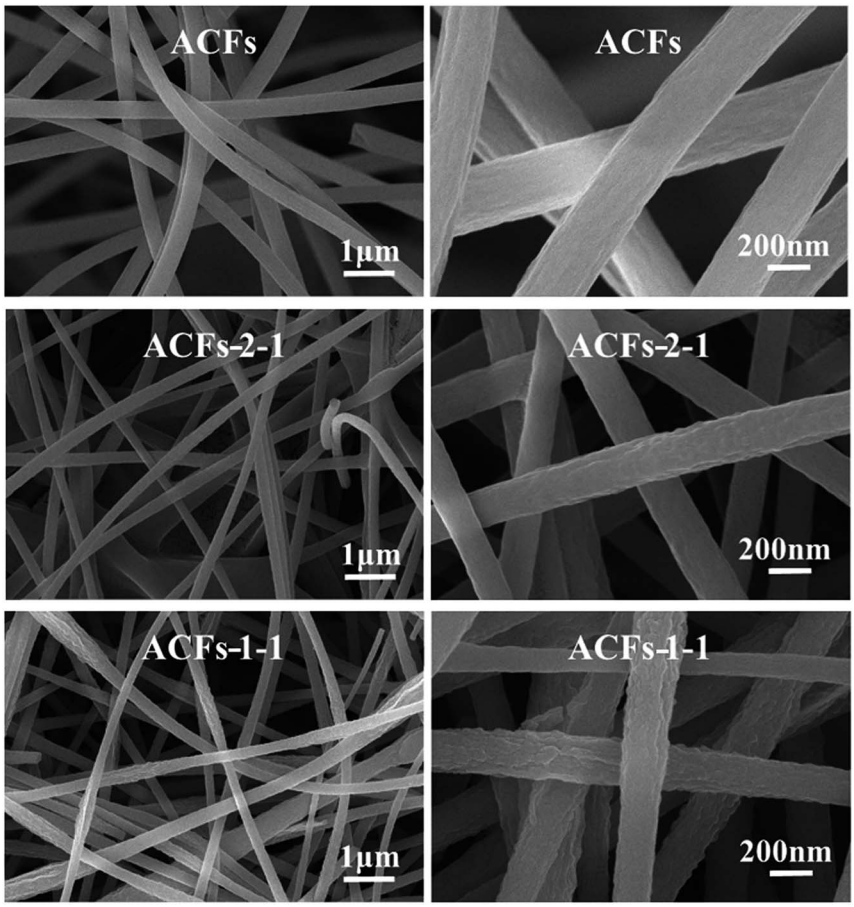

Fig. 3 SEM images of ACFs, ACFs-2-1, and ACFs-1-1 carbon fibers.

and 240 nm, respectively. The viscosity of the spinning solution has a significant impact on the diameter of the prepared fibers during the electrospinning process; lower viscosity can result in thinner fibers. In general, a decrease in molecular weight will cause reduction in the spinning solution viscosity.[33] In our previous study, it was found that the average molecular weight of Deposit was around 500, which was significantly lower than that of PAN. Furthermore, Deposit is mainly composed of aromatic molecules rather than chain structure molecules like PAN. Thus, when PAN was partly replaced by Deposit, the viscosity of the solution decreased and the average diameter of the carbon fibers showed a decreasing tendency. Moreover, the surface of ACFs-2-1 was rougher than that of ACFs; however, when the ratio reached 1 : 1, there were more obvious convex structure on the surface. All the obtained activated carbon fibers were flexible and could be folded easily; this ensured their direct use as supercapacitor electrodes.

Table 2 presents the specific surface area, total pore volume, and micro and mesopore volume of the activated carbon fibers. The specific surface areas of ACFs, ACFs-2-1 and ACFs-1-1 were 688, 1005, and 648 $m^2 g^{-1}$, respectively. The total pore volumes of the three activated carbon fibers were 0.33, 0.48, and 0.36 $cm^3 g^{-1}$, as presented in Table 2. These differences are related to the different weight loss ratios of PAN and Deposit during the stabilization and activation processes. It has been reported that the specific surface area of the electrospun carbon fibers activated by CO_2 ranges from 591 to 802 $m^2 g^{-1}$,[34–36] which is significantly lower than that of ACFs-2-1. These results show that the addition of Deposit significantly increases the specific surface area of the carbon fibers. When the ratio of PAN : Deposit reached 1 : 1, some micropores collapsed to mesopores or even macropores upon activation. This was proved by the fact that the mesopore volume increased from 0.05 $cm^3 g^{-1}$ to 0.09 $cm^3 g^{-1}$ with a decrease in the ratio; however, the specific surface area slightly decreased, as presented in Table 2.

Table 2 Surface properties of activated carbon nanofibers

Sample	Specific surface area ($m^2 g^{-1}$)	Total pore volume ($cm^3 g^{-1}$)	Pore volume ($cm^3 g^{-1}$)	
			Micropore	Mesopore
ACFs	688	0.33	0.26	0.05
ACFs-2-1	1005	0.48	0.40	0.05
ACFs-1-1	648	0.36	0.24	0.09

Fig. 4 displays the XRD spectra of the activated carbon nanofibers. The broad peak at around $2\theta = 24°$ implies the (002) crystallographic plane of graphite crystallites. When the ratio of PAN : Deposit increased, the peak intensity and width increased. In addition, the angle showed a slight shift to a higher degree. The crystallite size parameter L_C and the average interplanar spacing $d_{(002)}$ could be calculated by the Scherrer equation and Bragg equation, as shown below.[35]

$$L_C = \frac{0.89\lambda}{\beta \cos \theta} \quad (1)$$

$$d_{(002)} = \frac{\lambda}{2 \sin \theta} \quad (2)$$

Here, $\lambda = 0.154$ nm is the wavelength of the X-ray, θ is the scattering angle, and β is the half-width of the characteristic peaks in radian. Table 2 presents the surface properties of the activated carbon nanofibers.

Table 3 shows the calculated results of L_C and $d_{(002)}$. The $d_{(002)}$ values of the three activated carbon fibers were around 0.35 without significant difference. However, the L_C values showed an increasing tendency from 0.55 to 0.62 with the addition of Deposit. This implies that the addition of Deposit leads to more graphite crystallite planes.

Raman spectral analysis is also commonly used to measure the graphitization degree.[37] The Raman spectra of ACFs, ACFs-2-1 and ACFs-1-1 are shown in Fig. 4. In general, the Raman spectrum of a carbon material consists of two characteristic bands. The D-band centered at 1350 cm^{-1} is indicative of the defect-induced structures in graphene layers. The G-band at 1600 cm^{-1} is caused by ordered graphitic structures.[38] The R-value ($R = I_D/I_G$), indicating the amount of structurally ordered graphite crystallites, was calculated and presented in Table 3. With the addition of Deposit, the R value decreased from 1.70 to 1.38; this indicated that the structures of ACFs became more ordered with the addition of Deposit.

Simulation of the stabilization and activation of spun fibers

A thermogravimetric analyzer (TG) was used to simulate the processes of stabilization and activation of spun fibers. The

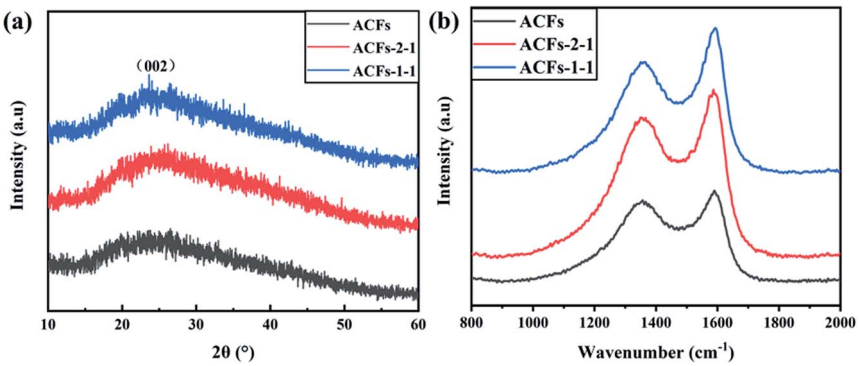

Fig. 4 (a) XRD patterns and (b) Raman spectra of ACFs, ACFs-2-1 and ACFs-1-1.

Table 3 XRD and Raman results of the prepared activated carbon fibers

	XRD				Raman
Sample	$2\theta_{(002)}$ (°)	β (radian)	L_c (nm)	$d_{(002)}$ (Å)	I_D/I_G
ACFs	24.51	0.26	0.55	0.35	1.70
ACFs-2-1	25.75	0.23	0.62	0.35	1.50
ACFs-1-1	25.20	0.24	0.60	0.35	1.38

temperature was increased to 280 °C at the heating rate of 0.5 °C min^{-1} and maintained at 280 °C for 2 h in air to stabilize the spun fibers. The temperature was then increased from 280 °C to 900 °C under an N_2 atmosphere at the heating rate of 5 °C min^{-1} for carbonization. Finally, the carrier gas was switched to CO_2, and the temperature was maintained at 900 °C for 1 h to activate the carbon fibers. The TG curves are shown in Fig. 5. It is obvious that the weight of the spun fibers decreases sharply when the temperature is increased to about 240 °C. This is mainly caused by the decomposition of PAN.[39] When PAN in the carbon fibers was partly replaced by Deposit, the weight loss at 240 °C declined significantly. The weight loss peaks at 240 °C, as shown in the DTG curves, also become smaller when the proportion of Deposit is increased. This implies that Deposit has better thermal stability than PAN. In our previous study, the softening point of Deposit has been found to be around 220 °C, which means that Deposit would slowly soften and coat the surface of the fibers. This may impede the decomposition of PAN. This caused the different weight loss behaviors of the three spun fibers during the stabilization process.

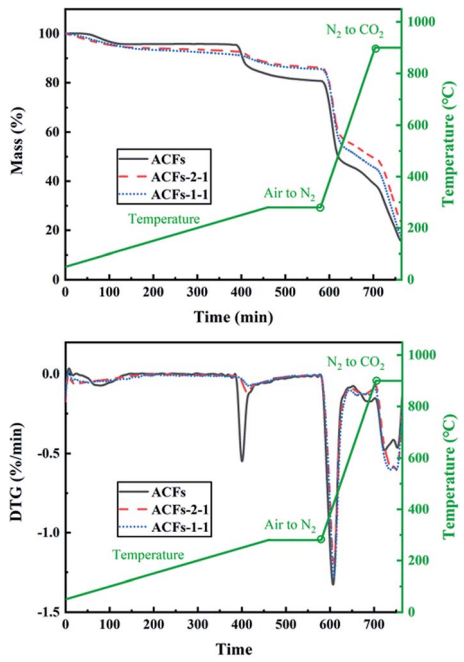

Fig. 5 TG and DTG curves of stabilization and activation simulation for the spun fibers.

When the temperature was increased from 280 °C to 900 °C under an N_2 atmosphere, the weight of the three carbon fibers decreased due to the dehydrogenation reaction and denitrification reaction. The residue weights of ACFs, ACFs-2-1 and ACFs −1 before activation were 38.52%, 49.36% and 45.48%, respectively. Moreover, the convex structure on the surface of ACFs-2-1 and ACFs-1-1 was formed, as shown in Fig. 3. These differences were caused by the differences in the carbon contents and thermochemical behaviors of PAN and Deposit. The DTG curves show that when the temperature is maintained at 900 °C, the peak caused by the reaction of CO_2 and carbon fibers becomes larger with the addition of Deposit. The weight losses of ACFs, ACFs-2-1 and ACFs-1-1 during the activation process were 23.07%, 26.12% and 27.82%, respectively. It was estimated that Deposit easily reacted with CO_2 and formed a porous structure. Thus, the micropore volume and specific surface area of ACFs-2-1 were higher than those of ACFs. However, the increase in the amount of Deposit may cause the collapse of some micropores to mesopores or even macropores, as discussed above.

Electrochemical characterization

The electrochemical characterization (CV, GCD, EIS and life cycling tests) of the activated carbon nanofibers was conducted by a three-electrode system in the potential range of −0.8–0.1 V using a 6 M KOH solution as an electrolyte. Fig. 6(a) presents the CV curves of ACFs, ACFs-2-1 and ACFs-1-1 at the scan rate of 5 mV s^{-1}. The CV curves of all the electrodes show a quasi-rectangular shape with a double-layer feature, and no obvious faradaic current is observed. In addition, the ACFs-2-1 and ACFs-1-1 electrodes displayed larger CV areas, suggesting their higher specific capacitance when compared with that of the ACF electrode. In general, the micropore and mesopore volumes are important factors for specific capacitance. Both micropores and mesopores provide adsorption sites for ions during the charge/discharge process.[40,41] Thus, due to the increased micropore volume and specific surface area of ACFs-2-1 and higher mesopore volume of ACFs-1-1, the specific capacitances of ACFs-2-1 and ACFs-1-1 were significantly higher than that of ACFs. Fig. 6(b) displays the CV curves of ACFs-2-1 at different scan rates. The CV curves exhibit a good quasi-rectangular shape at higher scan rates, and no obvious distortion can be observed, indicating a highly reversible system over the range of the potentials used herein.

Fig. 7(a) shows the GCD curves of the ACFs, ACFs-2-1 and ACFs-1-1 electrodes at the current density of 1 A g^{-1}. It is obvious that the charge–discharge curves of the three electrodes are almost linear and show a triangular shape, which indicates an ideal double-layer capacitive property. The specific capacitance of the three electrodes was directly calculated from the GCD curves by the following equation:

$$C = \frac{I\Delta t}{m\Delta V} \quad (3)$$

Here, I is the discharge current (A), Δt is the discharge time (s), m is the electrode weight (g), and ΔV is the potential range (0.9 V in this study). The calculated specific capacitances of the ACFs,

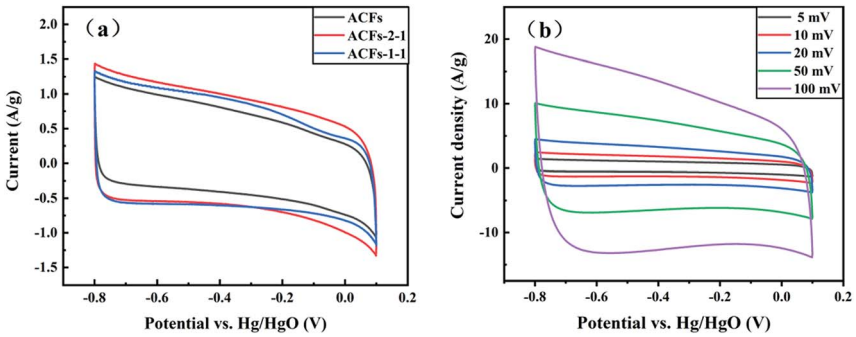

Fig. 6 CV curves of the (a) ACFs, ACFs-2-1, and ACFs-1-1 electrodes at the scan rate of 5 mV s^{-1} and (b) ACFs-2-1 electrode at different scan rates.

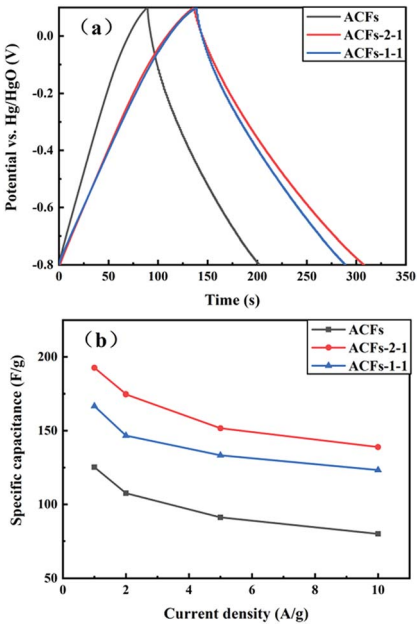

Fig. 7 Galvanostatic discharge curves of the ACFs, ACFs-2-1, and ACFs-1-1 electrodes at (a) 1 A g^{-1} and (b) different current densities from 1 to 10 A g^{-1}.

ACFs-2-1 and ACFs-1-1 electrodes were 125.2, 192.6 and 166.8 F g^{-1}, respectively. The result shows the same trend as the CV curves. This suggested that the introduction of Deposit could enhance the specific capacitance of electrodes.

To understand the high rate capability, GCD curves at different current densities ranging from 1 to 10 A g^{-1} were obtained (Fig. 7(b)). The increase in the current density caused diffusion limitation of electrolyte ions in the pore structure and resulted in decrease in the specific capacitance. With an increase in the current density from 1 to 10 A g^{-1}, the capacitance retention rates of the ACFs, ACFs-2-1 and ACFs-1-1 electrodes were 63.9%, 72.1% and 74.0%, respectively. The specific capacitance of an electrode at high currents is important for its practical application. The result demonstrated that the Deposit-based nanofiber had better high-rate handling capacity, suggesting the advantage of Deposit/PAN as an electrode material as compared to the case of pure PAN.

The EIS test was conducted to detect the charge and ion transport processes of the three electrodes. Fig. 8(a) shows the Nyquist plots of ACFs, ACFs-2-1 and ACFs-1-1. All the electrodes show a semicircular shape in the high-frequency region and a linear shape in the low-frequency region. This type of Nyquist plot indicates typical EDLC behavior.[42] The small semi-circle in the high-frequency region is generally attributed to the charge–discharge reaction process, and the diameter of the semi-circle represents the charge transfer resistance (R_{ct}). The R_{ct} values of ACFs, ACFs-2-1, and ACFs-1-1 were 1.74 Ω, 0.54 Ω, and 1.17 Ω, respectively. The intercept of the real axis also shows that ACFs-

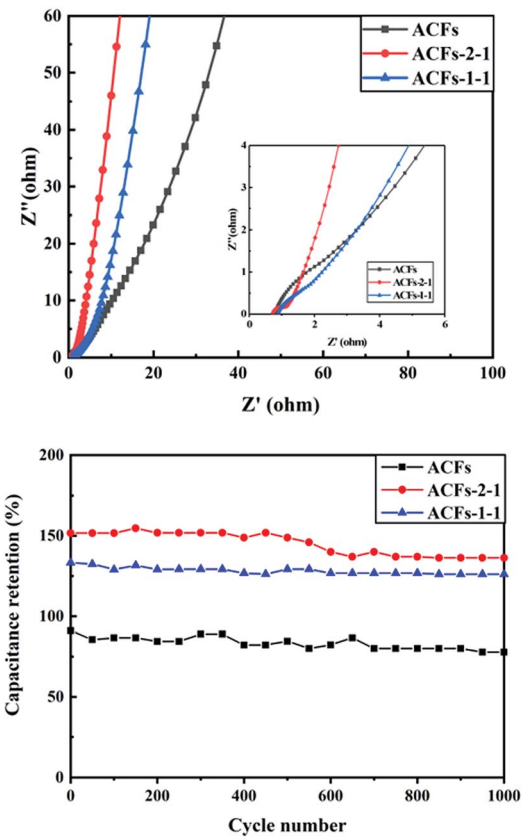

Fig. 8 Nyquist plots (a) and cycling stability of the (b) ACFs, ACFs-2-1, and ACFs-1-1 electrodes for 1000 cycles.

Table 4 Specific capacitance of the electrospun carbon nanofibers derived from coals reported in literature

Electrode Materials	Pretreatment	Electrolyte	Specific capacitance	Ref.
Acid-treated coal/PAN	Acid treatment with HNO_3 and H_2SO_4	6 M KOH	230 F g^{-1} (1 A g^{-1})	19
Oxidized coal/PAN	$KMNO_4$ as an oxidizing agent and H_2SO_4 as a solvent	6 M KOH	260 F g^{-1} (1 A g^{-1})	20
Coal liquefaction residues/PAN	Soxhlet extraction method using an *n*-hexane and toluene solution	6 M KOH	143 F g^{-1} (100 A g^{-1})	44
Acid-treated coal/PVA	Acid treatment with HNO_3 and H_2SO_4	6 M KOH	170 F g^{-1} (1 A g^{-1})	45
Deposit/PAN	Degradative solvent extraction	6 M KOH	193 F g^{-1} (1 A g^{-1})	This work

2-1 has the smallest equivalent series resistance (R_s). The slopes of the ACFs-2-1 and ACFs-1-1 electrodes are more vertical than that of the ACF electrode in the low-frequency region. The linear part reflects the ion transfer resistance, and an ideal vertical slope indicates pure capacitor-like behavior. The improved surface areas and pore structures of ACFs-2-1 and ACFs-1-1 lead to the reduction of these values, which is beneficial for improving the capacitive performance. In particular, the increased micropores and mesopores also cause good ion mobility in the intermediate regions. Lower resistance increases the current density at the electrode surface, thereby increasing the rate of ion diffusion to the electrode; this results in higher specific capacitance.

Fig. 8(b) displays the cycle-life test of ACFs, ACFs-2-1 and ACFs-1-1 at 5 A g^{-1} for 1000 cycles. The specific capacitance decreased during 1000 cycles, showing 14.6%, 10.2% and 5.4% decrease for ACFs, ACFs-2-1 and ACFs-1-1, respectively. This result indicated that no obvious structure change had occurred during the 1000-cycle-life test. Moreover, with the addition of Deposit, the electrodes displayed better cycling stability. The specific capacitances of the reported supercapacitors obtained using low-rank coal and its derived product by the electrospinning method are presented in Table 4. The specific capacitance ranged from 143 F g^{-1} to 260 F g^{-1}. In other cases, complex pretreatments, which required large quantities of valuable organic solvents or strong acids such as HNO_3 and H_2SO_4, impeded the practical use of supercapacitors. By comparison, the degradative solvent extraction used in this study is relatively simple and the extracted solvent can be easily recycled.[24,43] Moreover, the unextractable residue is upgraded coal, which can be used for activated carbon preparation and as a high-quality fuel for combustion and gasification.[26,27] All these factors indicate that Deposit has great potential as an excellent electrode material for supercapacitors.

Conclusions

In this study, low-rank coal was separated into three solid fractions by the degradative solvent extraction method. The high-molecular-weight extract (termed Deposit) had some characteristics similar to pitch but had narrower molecular weight range and better solubility in DMF. Thus, Deposit was used as a precursor for the preparation of activated carbon nanofibers, and we successfully prepared Deposit/PAN-based carbon nanofibers by electrospinning and CO_2 activation. Through thermogravimetric analysis, we found that Deposit and PAN displayed different thermal decomposition behaviors during the stabilization and activation processes. As a result, the specific surface area of the Deposit-based carbon nanofibers ACFs-2-1 increased from 688 m^2 g^{-1} to 1005 m^2 g^{-1} as compared to that of the ACFs obtained from pure PAN. Moreover, the specific capacitance of ACFs-2-1 was 192.6 F g^{-1}, whereas that of ACFs was only 122.8 F g^{-1} at 1 A g^{-1}. The retention rates of ACFs-2-1 and ACFs-1-1 were 89.8% and 94.6% after 1000 cycles, respectively. Therefore, this study proves that the thermal solvent extraction products of low-rank coal mixed with PAN are valuable precursors for the preparation of carbon nanofibers with excellent electrochemical properties.

Conflicts of interest

The authors declare that there is no conflict of interests regarding the publication of this article.

Acknowledgements

The National Natural Science Foundation of China (grant numbers 21776109, U1510119), the double first-class research funding of China-EU Institute for Clean and Renewable Energy (ICARE-RP-2018-BIOMASS-003), and the Foundation of State Key Laboratory of Coal Combustion (FSKLCCB1805) are gratefully acknowledged.

References

1 L. L. Zhang and X. S. Zhao, *Chem. Soc. Rev.*, 2009, **38**, 2520, DOI: 10.1039/b813846j.
2 S. Bose, T. Kuila, A. K. Mishra, R. Rajasekar, N. H. Kim and J. H. Lee, *J. Mater. Chem.*, 2012, **22**, 767–784, DOI: 10.1039/c1jm14468e.
3 J. Gamby, P. L. Taberna, P. Simon, J. F. Fauvarque and M. Chesneau, *J. Power Sources*, 2001, **101**, 109–116, DOI: 10.1016/s0378-7753(01)00707-8.
4 V. Presser, L. Zhang, J. J. Niu, J. McDonough, C. Perez, H. Fong and Y. Gogotsi, *Adv. Energy Mater.*, 2011, **1**, 423–430, DOI: 10.1002/aenm.201190015.
5 S. K. Simotwo, C. DelRe and V. Kalra, *ACS Appl. Mater. Interfaces*, 2016, **8**, 21261–21269, DOI: 10.1021/acsami.6b03463.
6 X. Mao, T. A. Hatton and G. C. Rutledge, *Curr. Org. Chem.*, 2013, **17**, 1390–1401, DOI: 10.2174/1385272811317130006.

7 X. Li, Y. Chen, H. Huang, Y.-W. Mai and L. Zhou, *Energy Storage Materials*, 2016, **5**, 58–92, DOI: 10.1016/j.ensm.2016.06.002.
8 S. Chaudhari, Y. Sharma, P. S. Archana, R. Jose, S. Ramakrishna, S. Mhaisalkar and M. Srinivasan, *J. Appl. Polym. Sci.*, 2013, **129**, 1660–1668, DOI: 10.1002/app.38859.
9 H. Wang, W. Wang, H. Wang, X. Jin, H. Niu, H. Wang, H. Zhou and T. Lin, *ACS Appl. Energy Mater.*, 2018, **1**, 431–439, DOI: 10.1021/acsaem.7b00 083.
10 C. Kim, B. T. N. Ngoc, K. S. Yang, M. Kojima, Y. A. Kim, Y. J. Kim, M. Endo and S. C. Yang, *Adv. Mater.*, 2007, **19**, 2341–2346, DOI: 10.1002/ad ma.200602184.
11 C. Kim and K. S. Yang, *Appl. Phys. Lett.*, 2003, **83**, 1216–1218, DOI: 10.1063/1.1599963.
12 T. D. Deepa, S. Mohapatra, S. V. Nair, A. S. Nair and A. Kumar Rai, *Sustainable Energy Fuels*, **1**, 138–144, DOI: 10.1039/C6SE00030D.
13 Q. Pan, N. Tong, N. He, Y. Liu, E. Shim, B. Pourdeyhimi and W. Gao, *ACS Appl. Mater. Interfaces*, 2018, **10**, 7927–7934, DOI: 10.1021/acsami.7b14498.
14 C. Kim, S.-H. Park, W.-J. Lee and K.-S. Yang, *Electrochim. Acta*, 2004, **50**, 877–881, DOI: 10.1016/j.electacta.2004.02.071.
15 A. G. Pandolfo and A. F. Hollenkamp, *J. Power Sources*, 2006, **157**, 11–27, DOI: 10.1016/j.jpowsour.2006.02.065.
16 K. S. Yang, C. Kim, S. H. Park, J. H. Kim and W. J. Lee, *J. Biomed. Nanotechnol.*, 2006, **2**, 103–105, DOI: 10.1166/jbn.2006.017.
17 S. H. Park, C. Kim, Y. O. Choi and K. S. Yang, *Carbon*, 2003, **13**, 2655–2657, DOI: 10.1016/S0008-6223(03)00272-0.
18 S. H. Park, C. Kim and K. S. Yang, *Synth. Met.*, 2004, **143**, 175–179, DOI: 10.1016/j.synthmet.2003.11.006.
19 H. Zhao, L. Wang, D. Jia, W. Xia, J. Li and Z. Guo, *J. Mater. Chem. A*, 2014, **2**, 9338–9344, DOI: 10.1039/c4ta00069b.
20 Y. He, L. Wang and D. Jia, *Electrochim. Acta*, 2016, **194**, 239–245, DOI: 10.1016/j.electacta.2016.01.19.
21 X. Li, R. Ashida and K. Miura, *Energy Fuels*, 2012, **26**, 6897–6904, DOI: 10.1021/ef301364p.
22 R. Ashida, M. Morimoto, Y. Makino, S. Umemoto, H. Nakagawa, K. Miura, K. Saito and K. Kato, *Fuel*, 2009, **88**, 1485–1490, DOI: 10.1016/j.fuel.2008. 12.003.
23 X. Li, X.-q. Zhu, L. Xiao, R. Ashida, K. Miura, G.-q. Luo and H. Yao, *J. Fuel Chem. Technol.*, 2014, **42**, 897–904, DOI: 10.1016/s1872 5813(14)60038-4.
24 X. Li, Z. Zhang, L. Zhang, X. Zhu, Z. Hu, W. Qian, R. Ashida, K. Miura, H. Hu, G. Luo and H. Yao, *Fuel Process. Technol.*, 2018, **173**, 48–55, DOI: 10.1016/j.fuproc.2018.01.005.
25 X. Li, D. E. Priyanto, R. Ashida and K. Miura, *Energy Fuels*, 2015, **29**, 3127–3133, DOI: 10.1021/ef502574b.
26 X. Li, R. Ashida, M. Makino, A. Nishida, H. Yao and K. Miura, *Energy Fuels*, 2014, **28**, 5690–5695, DOI: 10.1021/ef501305s.
27 Z. Zhang, Y. Xue, X. Zhu, X. Li, H. Yao and K. Miura, *Combustion behavior of low-rank coal upgraded by degradative solvent extraction*, The 8th International Symposium on Coal Combustion, Beijing China, 2015, DOI: 10.10 07/978-981-10-2023-0_4.
28 D. E. Priyanto, X. Li, R. Ashida and K. Miura, *Preparation of Activated Carbon from Extraction Residue of Low-Rank Coals, 19th Regional Symposium of Chemical Engineering*, Bali Indonesia, 2012.
29 J. Yang, K. Nakabayashi, J. Miyawaki and S.-H. Yoon, *Carbon*, 2016, **106**, 28–36, DOI: 10.1016/j.carbon.2016.05.019.
30 X. Ouyang, F. Wang, W. Sun, Z. Tao and F. Liu, *Hi-Tech Fiber Appl.*, 2018, **5**, 48–57.
31 F. Derbyshire, R. Andrews, D. Jacques, M. Jagtoyen, G. Kimber and T. Rantell, *Fuel*, 2001, **80**, 345–356, DOI: 10.1016/S0016-2361(0 0)00099-5.
32 I. Mochida, Y. Korai, C.-H. Ku, F. Watanabe and Y. Sakai, *Carbon*, 2000, **38**, 305–328, DOI: 10.1016/S0008-6223(99)00176-1.
33 R. M. Nezarati, M. B. Eifert and E. Cosgriff-Hernandez, *Tissue Eng., Part C*, 2013, **19**, 810–819, DOI: 10.1089/ten.tec.2012.0671.
34 Q. Dong, G. Wang, T. Wu, S. Peng and J. Qiu, *J. Colloid Interface Sci.*, 2015, **446**, 373–378, DOI: 10.1016/j.jcis.2014.12.065.
35 G. Wang, C. Pan, L. Wang, Q. Dong, C. Yu, Z. Zhao and J. Qiu, *Electrochim. Acta*, 2012, **69**, 65–70, DOI: 10.1016/j.electacta.2012.02.066.
36 M. Kim, Y. Kim, K. M. Lee, S. Y. Jeong, E. Lee, S. H. Baeck and S. E. Shim, *Carbon*, 2016, **99**, 607–618, DOI: 10.1016/j.carbon.2015.12.068.
37 M. Endo, C. Kim, T. Karaki, T. Kasai, M. J. Matthews, S. D. M. Brown, M. S. Dresselhaus, T. Tamaki and Y. Nishimura, *Carbon*, 1998, **36**, 1633–1641, DOI: 10.1016/s0008-6223(98)00157-2.
38 Y. Wang, S. Serrano and J. J. Santiago-Avilés, *Synth. Met.*, 2003, **138**, 423–427, DOI: 10.1016/s0379-6779(02)00472-1.
39 M. S. A. Rahaman, A. F. Ismail and A. Mustafa, *Polym. Degrad. Stab.*, 2007, **92**, 1421–1432, DOI: 10.1016/j.polymdegradstab.2007.03.023.
40 M. Zhi, F. Yang, F. Meng, M. Li, A. Manivannan and N. Wu, *ACS Sustainable Chem. Eng.*, 2014, **2**, 1592–1598, DOI: 10.1021/sc500336h.
41 C. Largeot, C. Portet, J. Chmiola, P.-L. Taberna, Y. Gogotsi and P. Simon, *J. Am. Chem. Soc.*, 2008, **130**, 2730–2731, DOI: 10.1021/ja7106178.
42 J. Chmiola, G. Yushin, Y. Gogotsi, C. Portet, P. Simon and P.-L. Taberna, *Science*, 2006, **313**, 1760–1763, DOI: 10.1126/science.1132195.
43 K. Miura, H. Nakagawa, R. Ashida and T. Ihara, *Fuel*, 2004, **83**, 733–738, DOI: 10.1016/j.fuel.2003.09.019.
44 X. Li, X. Tian, T. Yang, Y. He, W. Liu, Y. Song and Z. Liu, *ACS Sustainable Chem. Eng.*, 2019, **7**, 5742–5750, DOI: 10.1021/acssuschemeng.8b05210.
45 M. Guo, J. Guo, D. Jia, H. Zhao, Z. Sun, X. Song and Y. Li, *J. Mater. Chem. A*, 2015, **3**, 21178–21184, DOI: 10.1039/C5TA05743D.

